

High Temperature Oxidation Behaviors of SiON Coated AISI 441 in Ar+O₂, Ar+H₂O, and Ar+CO₂ Atmospheres

Kaustubh Bawane^a, Kathy Lu^{a*}, Quan Li^b, Rajendra Bordia^b

^aDepartment of Materials Science and Engineering, Virginia Polytechnic Institute and State University, Blacksburg, Virginia 24061, USA

^bDepartment of Materials Science and Engineering, Clemson University, Clemson, South Carolina 29634, USA

*Postal address: 117 Surge Building, 400 Stanger Street, Blacksburg, Virginia 24061

Email: klu@vt.edu (K. Lu)

Abstract

Silicon oxynitride (SiON) coated AISI 441 was prepared using pyrolysis of dip coated perhydropolysilazane (PHPS) precursor polymer. The high-temperature oxidation behaviors of SiON coated AISI 441 substrates were studied in Ar+O₂, Ar+H₂O, and Ar+CO₂ atmospheres at 800°C for 100 hours. The SiON coated AISI substrates showed better performance in all three atmospheres as compared to the uncoated AISI 441 substrate. This result is attributed to dense, crack free SiON coatings which provided complete separation between oxidizing species and the steel substrate. The thin oxide scale was observed on top of the SiON coating for all the atmospheres, which was attributed to the diffusion of metallic species (Cr, Mn, and Fe) in the AISI 441 substrate through the SiON coating.

Keywords: oxidation resistant coating; SiON; ferritic stainless steel; diffusion; atmosphere

1. Introduction

Damage due to oxidation of metals during high-temperature use in aggressive environments causes billions of dollars of economic loss every year. Protective ceramic coatings have been contributing towards improving high temperature oxidation resistance of metals for a long time [1, 2]. Such protective coatings should possess high resistance to aggressive atmospheres, high density, excellent bonding to metal substrate, good microstructural and thermal stability, and resistance to cracking during high temperature service [3, 4]. A number of expensive techniques such as physical vapor deposition (PVD), chemical vapor deposition (CVD), and thermal spray are routinely used to produce thermal barrier coatings (TBCs) and/or environmental barrier coatings (EBCs) for a variety of high temperature applications [1, 5, 6].

In recent years, polymer derived ceramics (PDCs) have evolved as an economical and easy-to-process alternative to produce ceramic coatings [1, 7, 8]. In this method, relatively inexpensive techniques such as dip coating, spin coating, and spray coating are used to coat polymeric precursors (organoelemental compound – mostly silicon-based such as polysilazanes) on substrates [7, 9-13]. The precursor coatings can be converted into desired ceramics using pyrolysis at elevated temperatures. PDC coatings offer a wide range of tailorable attributes. Microstructures, phases, and thereby properties can be tailored by using different pyrolysis atmospheres, temperatures, and a large selection of precursors [1, 5, 6, 8]. Previous literature indicates polymer derived ceramics possess excellent high temperature stability and oxidation resistance [14-17]. A variety of polymer derived ceramic coatings such as SiOC [6, 18, 19], SiCN [8, 12], and SiON [5, 12] have been investigated in order to improve the corrosion and oxidation resistance of metallic substrates.

Silicon oxynitride (SiON) coatings are widely used for a variety of applications such as anti-reflection coatings in solar cells [20], gas barrier films for food/medical packaging systems [21], and corrosion and oxidation resistant coatings [12, 22, 23]. Recently, magnetron sputtered SiON nano-films (~80 nm) have been developed for corrosion and high temperature oxidation resistance of motorcycle exhaust systems [22]. In most of these applications, SiON ceramic was deposited using expensive sputter coating, plasma-enhanced CVD, and PVD methods [20-22]. Recently, dense and crack-free amorphous SiON coating was successfully fabricated using pyrolysis of PHPS precursor at high temperatures in an air atmosphere [6, 24-26]. SiON coatings consist of a thin layer of SiO₂ on the outer surface which forms during pyrolysis in air. This layer is impermeable to most of the oxidizing species [1, 27].

Wang et al. [6] studied high temperature oxidation behaviors of SiON coated Inconel 617 superalloy in air atmosphere. The SiON coating was able to provide excellent protection against oxidation up to 200 hours at 800°C. The oxidation response of SiOC coated Inconel 617 with a SiON bond coat layer was also studied. The SiON bond coat layer successfully prevented the formation of the thermally grown oxide layer at the coating-substrate interface as opposed to SiOC coated Inconel 617 without any bond coat [6, 24]. Riffard et al. [5] reported significant improvement in the oxidation resistance of AISI 304 stainless steel at 900°C in air atmosphere as a result of PHPS derived SiON coating. Gunthner et. al. [1] also showed excellent oxidation performance of SiON coated AISI 304 stainless steel up to 1000°C in air atmosphere. TEM studies revealed excellent adhesion between SiON coating and AISI 304 substrate as a result of the interdiffusion layer at the interface [1]. The previous literature on SiON coatings reports oxidation in mostly air atmosphere [1, 5, 24]. In various aggressive industrial atmospheres, exhaust systems, and solid oxide cells, oxidizers such as H₂O and CO₂ co-exist with O₂. The performance of SiON

coated metallic substrates in various aggressive oxidizing conditions such as H₂O and CO₂ is still unknown.

In this work, high-temperature oxidation behaviors of SiON coated AISI 441 ferritic stainless steel substrates under aggressive Ar+O₂, Ar+H₂O and Ar+CO₂ environments have been studied. A variety of characterization techniques, including X-ray diffraction (*XRD*), scanning electron microscopy (*SEM*), energy dispersive X-ray spectroscopy (*EDS*) in scanning transmission electron microscopy (*STEM*), and X-ray photoelectron spectroscopy (*XPS*) have been employed to elucidate the interaction between the coating and the substrate and the oxidation mechanisms of SiON coated AISI 441 steel under these atmospheres.

2. Materials and methods

In this study, AISI 441 ferritic stainless steel substrates were used for polymer derived ceramic (PDC) coating deposition. The substrates (10 mm L×5 mm W×1 mm H) were polished with 1200 SiC grit polishing papers. The fine polishing was performed using a 1 μm alumina solution. Silicon oxynitride (SiON) coating was obtained on AISI 441 using a dip coating method (need input from Clemson on the dip coating equipment name and dip coating conditions). PHPS (Clariant Advanced Materials GmbH, Sulzbach, Germany) was used as a polymer precursor solution for dip coating. The crosslinking was carried out at 150°C. The pyrolysis was carried out at 800°C with heating/cooling rates of 2°C/min and a holding time of 2 hours. Both ends of the tube furnace (CM-1200, CM Furnace Inc., Bloomfield, NJ, USA) were kept open to ensure the exposure of the samples to flowing air. The final thickness of the SiON coating was around 0.8-1 μm.

SiON coated AISI 441 substrates were thermally treated at 800°C for 100 hours in the following different atmospheres: Ar + 20% CO₂, Ar + 20% H₂O, and Ar +20% O₂ (hereafter referred as Ar +CO₂, Ar+H₂O, and Ar+O₂ respectively). The thermal treatments were performed in a tube furnace (1730-20 HT Furnace, CM Furnace Inc., Bloomfield, NJ, USA). The flow rate for the above-mentioned gas mixtures was ~1.2 L·min⁻¹ at 1 atm pressure. The Ar+H₂O mixture was obtained by heating a water container at 60°C and then introducing industrial grade argon gas through it before passing the mixture through the tube furnace. The other gas mixtures were provided by Airgas Inc, Christiansburg, VA, USA.

Phase composition analysis was carried out using an X-ray diffractometer (PANalytical B.V., Almelo, Netherlands) with Cu-K α radiation at an operating condition of 45 kV/40 mA. Surface composition analysis was carried out using *XPS* (PHI Quantera SXM, Chanhassen, MN, USA). The baseline correction and background subtraction of *XPS* survey plots were carried out using OriginPro 8.5 software. CASAXPS software was used for identification and quantification of elements from *XPS* data. Surface morphology and cross-section microstructure analyses were performed using scanning electron microscopy (FEG E-SEM QUANTA600, FEI Company, Hillsboro, OR, USA) and energy dispersive spectroscopy (BRUKER EDS). Cross-section STEM-EDS analysis was performed to identify oxide layer compositions (JEOL 2100, Peabody, MA, USA). The TEM sample was prepared using a focused ion beam (FIB) lift-out technique (Helios 600 Nanolab focused ion beam, FEI Company, Hillsboro, OR, USA).

3. Results

3.1 Oxide layer thickness

In this work, the oxide layer thickness is used as a tool to evaluate the effect of the SiON coating on the oxidation resistance performance of the AISI 441 substrate. The thickness data in Fig. 1 indicate that the SiON coating has led to significant improvement in the oxidation resistance of AISI 441 in all atmospheres. After the thermal treatment in the Ar+CO₂ atmosphere, the SiON coated AISI 441 samples show around 90% reduction in the oxide layer thickness as compared to the uncoated AISI 441 (0.24±0.07 μm vs. 2.45±0.4 μm respectively). In Ar+H₂O, the oxide layer thickness of the SiON coated AISI 441 sample is 76% smaller than that of the uncoated AISI 441 (0.55±0.08 μm vs. 2.34±0.36 μm). In the Ar+O₂ atmosphere, the SiON coated AISI 441 shows 80% decrease in the oxide layer thickness as compared to the uncoated AISI 441 (0.44±0.14 μm vs. 2.25±0.53 μm). The oxide layer thickness data in Fig. 1 show that the thermal treatment in different atmospheres (i.e. Ar+CO₂, Ar+H₂O, and Ar+O₂) has little effect on the oxidation resistance of the uncoated AISI 441. In contrast, the SiON coated AISI 441 samples show the highest oxidation for the Ar+H₂O samples (0.55±0.08 μm) followed by the sample treated in Ar+O₂ atmosphere (0.44±0.14 μm) and the lowest damage for the Ar+CO₂ (0.24±0.07 μm) sample. This means that Ar+H₂O is the most aggressive atmosphere in the oxidation of the SiON coating.

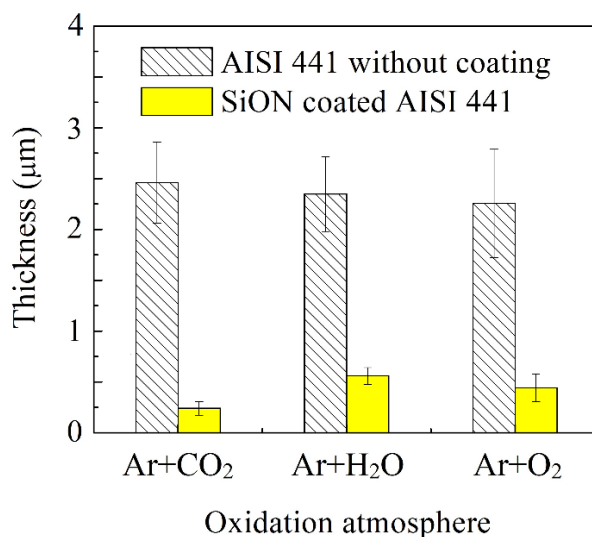


Fig. 1. Effect of atmosphere on the oxide layer thickness on AISI 441 (a) without coating and (b) with the SiON coating after the thermal treatment at 800°C for 100 hours.

3.2 Phase composition

Figs. 2a and 2b show the XRD patterns of the uncoated AISI 441 and SiON coated AISI 441 samples respectively after the thermal treatment in Ar+CO₂, Ar+H₂O, and Ar+O₂. The XRD pattern of the uncoated AISI 441 reveals the presence of Cr₂O₃ and (Mn, Cr, Fe)₃O₄ phases along with the steel (α -ferrite) substrate for all the atmospheres as shown in Fig. 2a. The XRD patterns of the SiON coated AISI 441 after the thermal treatment in Ar+H₂O and Ar+O₂ atmospheres indicate a similar mixture of Cr₂O₃ and (Mn, Fe, Cr)₃O₄ phases along with the peaks from the AISI441 steel. In contrast, the XRD pattern of the SiON coated AISI 441 after the treatment in Ar+CO₂ shows only the steel peaks. This result correlates well with the very small oxide thickness ($0.24 \pm 0.07 \mu\text{m}$) of the sample treated in Ar+CO₂ as compared to that of Ar+H₂O and Ar+O₂ (see Fig. 1).

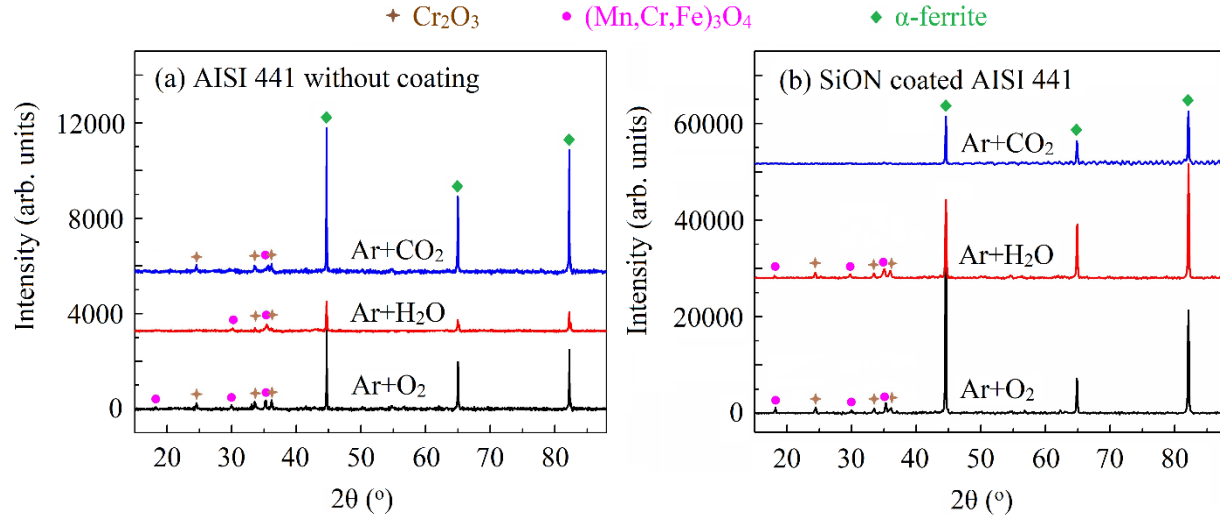


Fig. 2. XRD patterns of AISI 441: (a) without coating, (b) with SiON coating, after the thermal treatment at 800°C in Ar+CO₂, Ar+H₂O, and Ar+O₂ atmospheres for 100 hours.

3.3 Surface morphology

Figs. 3a and 3d show the oxidized surface morphology of the AISI 441 substrates without any coating and with the SiON coating after the thermal treatment in Ar+CO₂. The substrates without a coating show a mixture of thicker and thinner areas as shown in Fig. 3a. The thicker areas are likely along grain boundaries. This is believed to be due to higher diffusion rates for both oxygen and metal ions through grain boundaries, which can lead to more aggressive attack locally. With the metal oxide formation, there is a volume expansion, which causes the ridge-like features. The SiON coated substrates show a much smoother morphology (see Fig. 3). Figs. 3b and 3e show the oxidized layer morphology of the Ar+H₂O treated substrates (without and with the SiON coating respectively). The uncoated AISI 441 substrate shows a highly porous morphology, indicative of high oxidation damage. Such porous morphology is caused by the volatile reaction products (e.g. chromium hydroxides), which is commonly observed with the loss of Cr₂O₃ on top

of high Cr steels in a water vapor containing atmosphere. On the other hand, the surface morphology of the SiON coated samples is dense and devoid of any cracks or pores. This means that the SiON coating can effectively suppress the formation of volatile reaction products. Figs. 3c and 3f show the oxide layer morphology of the AISI 441 substrate with and without the SiON coating after the Ar+O₂ treatment respectively. The uncoated AISI 441 in Fig 3c shows faceted crystals on the surface, which are believed to be spinel type (Mn,Cr,Fe)₃O₄ as confirmed by the XRD result in Fig. 2a. In contrast, the SiON coated AISI 441 substrate shows fine hemispherical island-like morphology on the surface (see Fig. 3f). This indicates that even though oxidation products are the same for the AISI samples with and without the SiON coating, the mechanism of oxidation is significantly different.

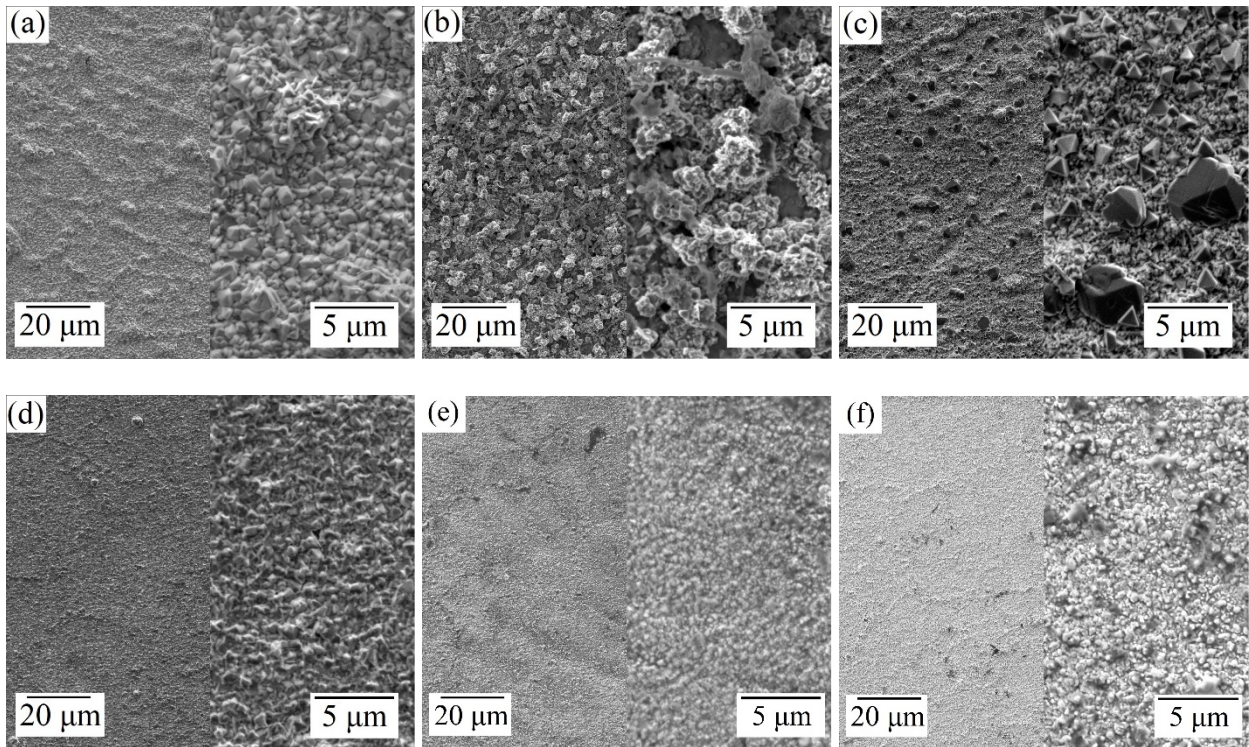


Fig. 3. Surface morphology after the thermal treatment at 800°C for 100 hours: AISI 441 without

any coating in (a) Ar+CO₂, (b) Ar+H₂O, (c) Ar+O₂; and AISI 441 with the SiON coating in (d) Ar+CO₂, (e) Ar+H₂O, and (f) Ar+O₂ atmospheres.

3.4 Oxide layer evolution

Figs. 4a and 4b shows the cross-section SEM images and corresponding EDS maps of the SiON coated AISI 441 substrates after the thermal treatment in the Ar+CO₂ and Ar+O₂ atmospheres respectively. The SEM image of the sample treated in the Ar+CO₂ atmosphere (Fig. 4a) shows an intact SiON coating along with a very thin layer of oxide on top as seen in the magnified image in the upper left corner. On the other hand, the SEM image of the sample treated in Ar+O₂ shows an intact SiON layer with a slightly thicker oxide layer on top as demonstrated in the upper left corner of Fig 4b. The EDS maps for both the Ar+CO₂ and Ar+O₂ samples (Fig. 4a and 4b respectively) show that the Cr element has diffused through the coating and formed an outer oxide layer while the Fe element ends exactly at the baseline of the coating (yellow dotted line). The silicon EDS maps in Figs. 4a and 4b confirm that the SiON coating is devoid of cracks or damage. The oxygen-rich layer for both Ar+CO₂ and Ar+O₂ is slightly thicker than the Si-rich layer, therefore compromising the SiON coating.

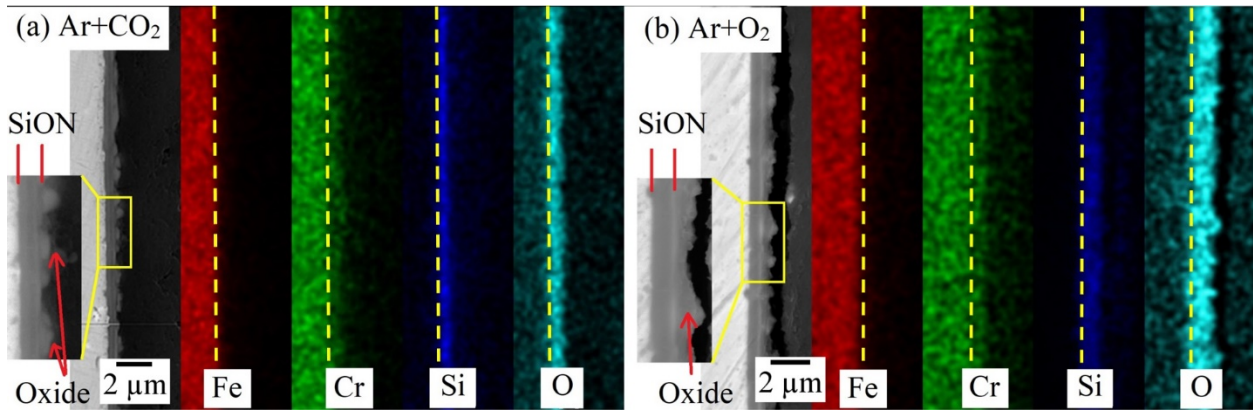
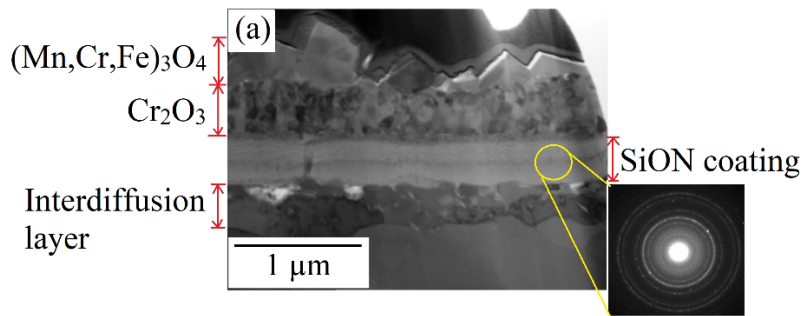


Fig. 4. EDS maps of the SiON coated AISI 441 after the thermal treatment at 800°C for 100 hours in (a) Ar+CO₂ and (b) Ar+O₂ atmosphere.

STEM-EDS analysis results of the SiON coated AISI 441 treated in Ar+H₂O are shown in Figs. 5a and 5b. Fig. 5a confirms the presence of the fully intact and well bonded amorphous SiON coating. The EDS mapping results in Fig. 5b show that the topmost oxide layer is rich in Mn, Fe, and Cr. The second layer is rich in Cr and O. These correlates well with the presence of (Mn,Cr,Fe)₃O₄ and Cr₂O₃ peaks in the XRD pattern in Fig. 2b. The topmost (Mn,Cr,Fe)₃O₄ layer is discontinuous with varying thickness. The second Cr₂O₃ layer is continuous without any cracks or porosity. This means that Cr, Mn and Fe have diffused through the amorphous SiON coating during the thermal treatment and reacted with the respective atmosphere (CO₂, H₂O, and O₂) to form a layered oxide structure. The STEM bright field image in Fig. 5a reveals the interdiffusion layer between the SiON coating and the steel substrate. This interdiffusion layer ensures strong bonding between the SiON coating and the steel, therefore protects the steel from direct contact with the oxidizing atmospheres.



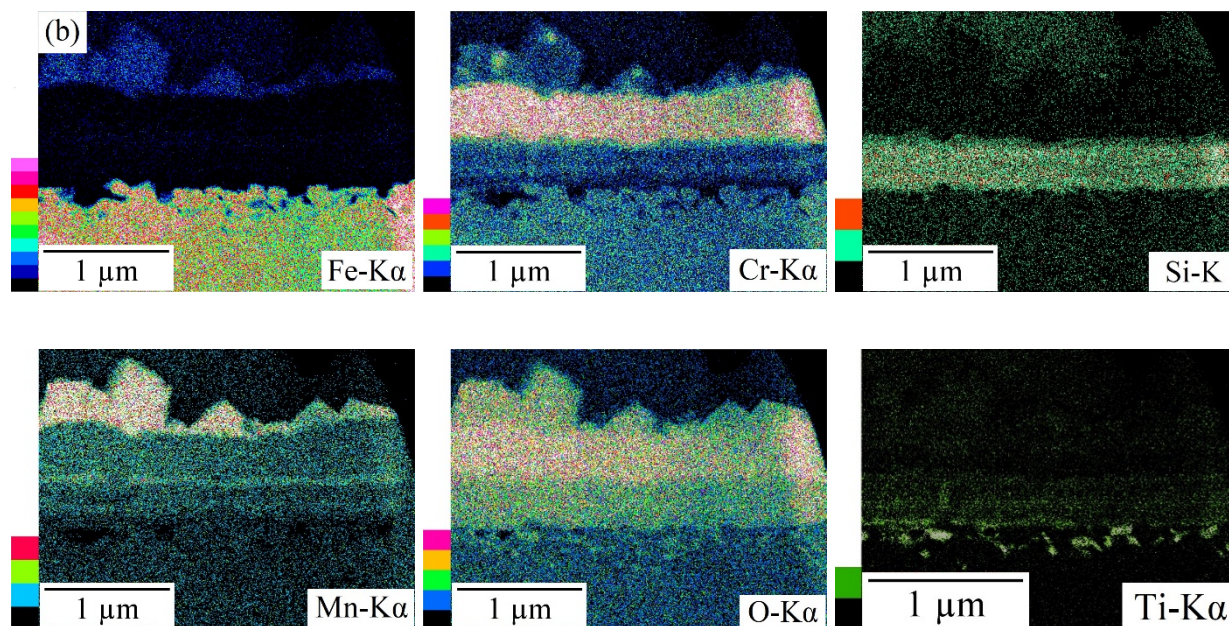


Fig. 5. (a) Cross-section BF-STEM image and corresponding (b) EDS maps of the SiON coated AISI 441 after the thermal treatment at 800°C for 100 hours in Ar+H₂O atmosphere.

Figs. 6a and 6b show the XPS surface analysis results of the SiON coated AISI 441 treated in the Ar+H₂O and Ar+O₂ atmospheres respectively. The sample treated in Ar+O₂ shows strong Si peaks (Fig. 6b) as opposed to that in Ar+H₂O (Fig. 6a). Table 1 shows surface elemental compositions (atom %) calculated using the CASAXPS software. The XPS data show a much higher concentration of Si after the Ar+O₂ treatment as compared to the Ar+H₂O treatment (40.04 at% vs. 5.7 at%). This indicates that unlike the Ar+H₂O treated sample, the top SiO₂ layer on the SiON coating is exposed and not entirely covered by the metal oxides. This result correlates well with the SEM surface morphology in Fig. 3f and the cross-section SEM-EDS results in Fig. 4b where the top Cr- and Mn-rich oxide layer is in the form of islands and not a continuous layer. At the same time, the BF-STEM image of the Ar+H₂O treated sample shows that almost the entire sample is covered with the metal oxides, consistent with the strong Mn and Cr peaks in Fig. 6a.

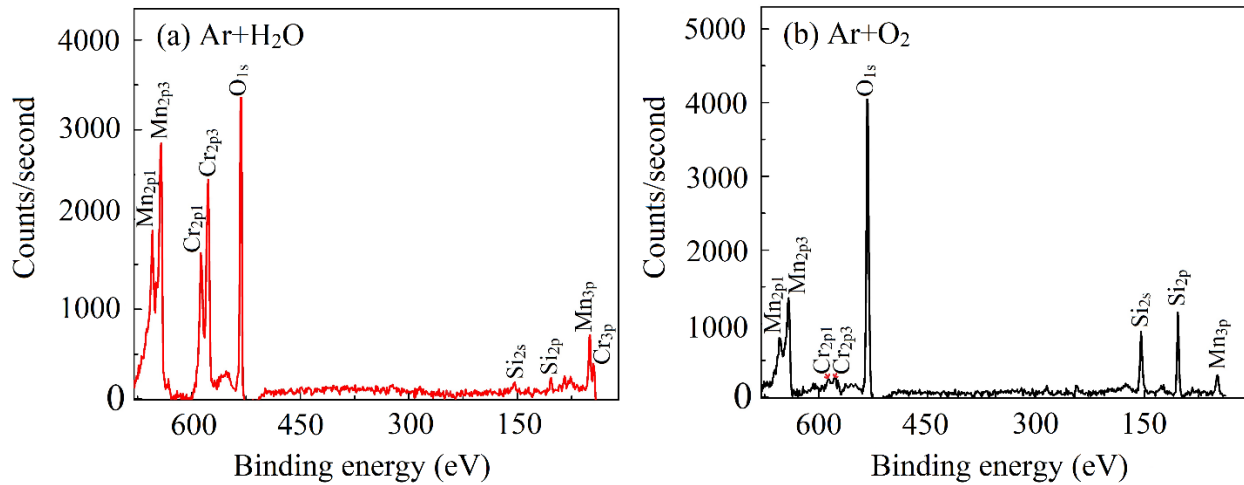


Fig. 6. XPS surface analysis results of the SiON coated AISI 441 after the thermal treatment at 800°C for 100 hours in (a) Ar+H₂O and (b) Ar+O₂ atmospheres.

Table 1. Surface elemental compositions from the XPS analysis (in atomic %).

Elements	O 1s	Si 2p	Cr 2p	Mn 2p
Ar+H ₂ O	53.46	5.72	20.53	20.29
Ar+O ₂	51.57	40.04	1.11	7.28

4. Discussion

The reaction in equation 1 describes the oxidation of the metal species in AISI 441 as a result of exposure to oxidizing atmospheres at elevated temperatures. The rate of this reaction depends on the ability of the metallic species diffusing to the oxide-scale interface as well as the ability of oxygen diffusing to the oxide-metal interface [28, 29]. In case of fast diffusion of both oxygen and metal species through the scale, the rate of oxidation will be high.



The STEM-EDS results of the SiON coated AISI 441 treated in Ar+H₂O indicate that the oxide scales only appear above the coating (Fig. 5) while there is no indication of oxidation at the coating-steel interface. The interdiffusion layer indicates strong bonding between the SiON coating and the AISI 441 substrate. The SEM-EDS results of the SiON coated AISI 441 treated in Ar+CO₂ in Fig. 4 show small island-like oxide structures above the intact and well-bonded SiON coating. This means that the oxidation of the SiON coated AISI 441 is mainly governed by the diffusion of the metallic species through the SiON coating and oxide scale towards the oxide-gas interface. While the SiON coating has been successful in preventing diffusion of the oxidizing species in all atmospheres, mainly due to the impermeable SiO₂ top layer (green layer in Fig. 7a), this explanation is supported by a significant reduction in the oxide thickness in the SiON coated AISI 441 as compared to the uncoated AISI 441 in all the atmospheres: Ar+CO₂, Ar+H₂O, and Ar+O₂ as shown in Fig. 1. Therefore, the SiON coating is effective in thwarting the diffusion of the oxidizers but allows moderate diffusion of the metallic species (Cr, Mn, and Fe). Fig. 7a shows a schematic representation of the oxidation resistance improvement as a result of complete separation between the oxidizing environments and the AISI 441 steel due to the SiON coating.

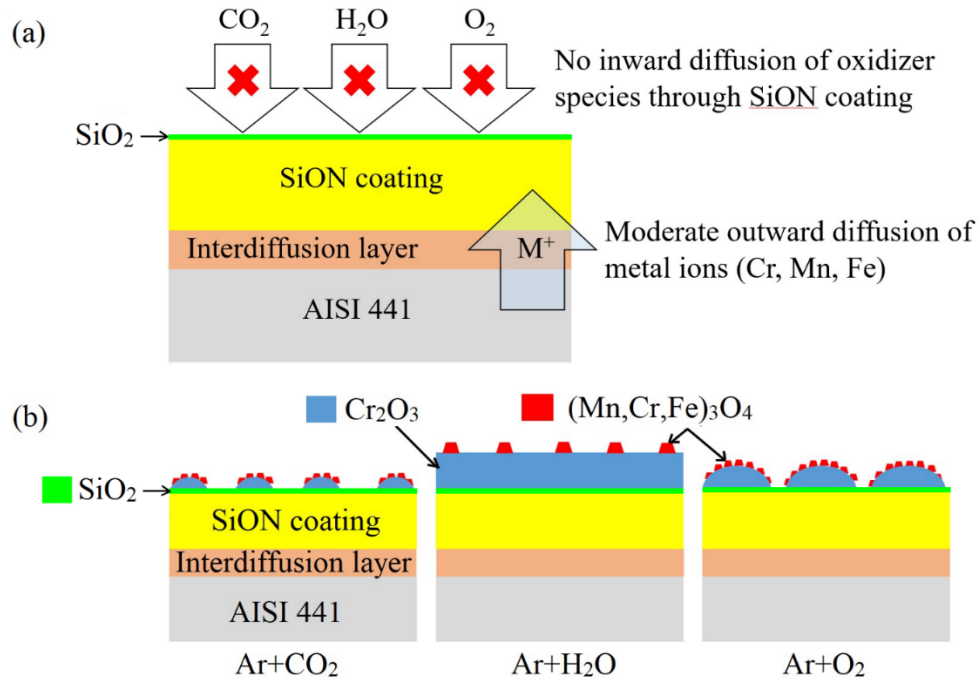
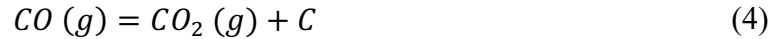
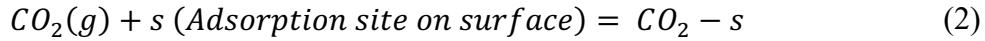


Fig. 7. Schematic representation of the coating microstructure, (a) after pyrolysis at 800°C in an oxidizing atmosphere for 2 hours, (b) after thermal treatment at 800°C for 100 hours in Ar+CO₂, Ar+H₂O, and (c) Ar+O₂ atmospheres respectively.

Fig. 7b shows a schematic representation of the oxidation behaviors of the SiON coated AISI 441 steel in CO₂, H₂O, and O₂ containing atmospheres. The SiON coated AISI 441 treated in the Ar+CO₂ atmosphere shows a surface morphology with small island-like oxides. This means that some top SiO₂ layer of the SiON coating is still exposed. During the thermal treatment, the CO₂ gas molecules adsorb on the SiON surface and dissociate into oxygen ions and CO gas according to equations 2 and 3 respectively [28-30]. The adsorbed oxygen ions can react with diffusing metal species such as Cr, Mn, and Fe and form a layer of Cr₂O₃ topped with (Mn,Cr,Fe)₃O₄ spinel oxides. In the case of uncoated AISI 441, CO can convert back to CO₂ per reaction 4, especially at the metal-coating interface where the oxygen potential is lowest. The C

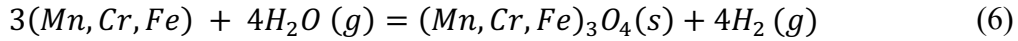
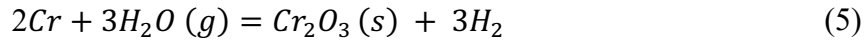
released through reaction 4 can dissolve in the AISI 441 metal or precipitate as carbides just underneath the oxide scale. For the SiON coated substrate, the complete separation between the atmosphere and the metal substrate can effectively prevent the carburization or carbide precipitation, which is common for the oxidation process under a CO₂-containing atmosphere.



The TEM results in Fig 5 and the schematic drawing in Fig. 7b shows the presence of a continuous Cr₂O₃ layer topped with a discontinuous (Mn,Cr,Fe)₃O₄ spinel phase above the intact SiON coating after the thermal treatment in the Ar+H₂O atmosphere. We believe that the water vapor reacts with the diffusing metallic species (Cr, Fe, and Mn) according to reactions given in equations 5 and 6. The reaction between Cr₂O₃ and water vapor further leads to the formation of volatile chromium hydroxides. For the uncoated AISI 441, these volatile chromium hydroxides can damage the protective Cr₂O₃ layer and expose the underlying substrate to oxidation, which can also trigger ‘breakaway oxidation’ when the supply of Cr to the surface becomes insufficient to sustain continuous rebuilding of the protective Cr₂O₃ layer. The volatile product also leads to cracks and a porous oxide structure, which is evident for the uncoated AISI 441 sample treated in Ar+H₂O as shown in Fig. 3b. On the other hand, for the SiON coated AISI 441, the volatile chromium hydroxide cannot expose the steel surface and further deterioration of the substrate is prevented.

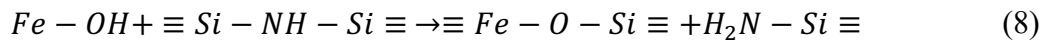
The higher oxidation damage for the SiON coated AISI 441 treated in Ar+H₂O as compared to Ar+CO₂ can be seen in the thickness data in Fig. 1. This behavior is not observed in the uncoated AISI 441 in which the oxide thickness is almost similar for all the atmospheres (in fact, marginally higher for the Ar+CO₂ treated sample). As known, the oxidation reaction at the

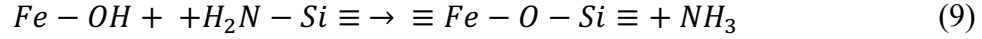
coating/gas interface starts with the adsorption of H₂O or CO₂ on the coating surface [28, 29], the top SiO₂ layer on the SiON coating is hydrophilic [24]. In addition, SiO₂ and CO₂ are very stable species. Thus, the hydrophilic nature of the top SiO₂ layer can help adsorb H₂O molecules on the surface better. This explains higher oxidation damage and fully covered oxide layer for the Ar+H₂O treated samples. Another possible interaction between the top SiO₂ layer and water vapor includes reaction between them to form volatile Si(OH)₄ species (see equation 7) [31-33]. Such interactions can make Ar+H₂O more aggressive than Ar+CO₂ for the SiON coated AISI 441.



The schematic drawing of the oxidation behavior of the SiON coated AISI 441 in Ar+O₂ is shown for the last case in Fig. 7b. The presence of Cr₂O₃ and (Mn,Cr,Fe)₃O₄ is commonly observed for AISI 441 treated in air or O₂ atmosphere [34, 35]. The XPS results in Fig. 6b and Table 1 show a considerable amount of Si and a low amount of Cr. This means that the oxides have not achieved full surface coverage as in the case of the Ar+H₂O treated sample. The low amount of Cr indicates that the Mn-rich spinel (Mn,Cr,Fe)₃O₄ probably forms a continuous layer covering the Cr₂O₃ oxide, unlike the case for the Ar+H₂O treated sample.

One of the important aspects contributing towards the high oxidation resistance is the excellent adhesion between the SiON coating and the AISI 441 substrate. The adhesion can result from direct chemical bonding as a result of the reaction between the SiOC and the metal hydroxides present on the AISI 441 surface as shown in equations 8 and 9 [1, 36]. The SiON-steel bonding is supported by strong interdiffusion layer as shown in the STEM image in Fig. 5.





Overall, the SiON coating is a strong barrier for aggressive oxidizing species such as CO₂, H₂O, and O₂. The limited AISI 441 degradation is mainly attributed to the outwards diffusion of the metallic species through the SiON coating layer. In the future, a double-layered coating can be engineered, where the inner layer is capable of thwarting Cr, Mn, and Fe diffusion while the dense and crack-free SiON layer can prevent the inward diffusion of aggressive oxidizers. Even in its current form, the SiON coating is successful in achieving significant improvement in the oxidation resistance of AISI 441.

5. Conclusions

In this work, AISI 441 substrates with and without SiON coating have been thermally treated at 800°C for 100 hours in Ar+O₂, Ar+H₂O, and Ar+CO₂ atmospheres. Oxidation damage in the SiON coated AISI 441 is significantly less than that in the uncoated AISI 441 substrate. The improved oxidation resistance is attributed to the complete separation between the AISI 441 steel substrate and the oxidizing gases due to the SiON coating. The excellent bonding between SiON and the steel is attributed to direct chemical bonding as well as the formation of an interdiffusion layer. The oxide layer observed on top of the intact SiON layer for all the atmospheres is due to moderate diffusion of Cr, Fe, and Mn elements through the SiON coating and the interdiffusion layer. Overall, the SiON coating is effective in enhancing the oxidation resistance of AISI 441.

Acknowledgment: KB and KL acknowledge the financial support from National Science Foundation under grant number CMMI-1634325. RKB and QL acknowledge financial support from the Department of Energy under grant number DE-FE0031281.

Conflict of Interest

The authors declare that they have no conflict of interest.

References

- [1] M. Günthner, T. Kraus, A. Dierdorf, D. Decker, W. Krenkel, G. Motz, Advanced coatings on the basis of Si(C)N precursors for protection of steel against oxidation, *Journal of the European Ceramic Society*, 29 (2009) 2061-2068.
- [2] J.D. Torrey, R.K. Bordia, Processing of Polymer-Derived Ceramic Composite Coatings on Steel, *J Am Ceram Soc*, 91 (2007) 41-45.
- [3] K.N. Lee, Current status of environmental barrier coatings for Si-based ceramics, *Surf Coat Tech*, 133 (2000) 1-7.
- [4] Y. Dong, K. Ren, Y. Lu, Q. Wang, J. Liu, Y. Wang, High-entropy environmental barrier coating for the ceramic matrix composites *Journal of European Ceramic Society*, 39 (2019) 2574-2579.
- [5] F. Riffard, E. Joannet, H. Buscail, R. Rolland, S. Perrier, Beneficial Effect of a Pre-ceramic Polymer Coating on the Protection at 900 °C of a Commercial AISI 304 Stainless Steel, *Oxidation of Metals*, 88 (2017) 211-220.
- [6] K. Wang, M. Günthner, G. Motz, R.K. Bordia, High performance environmental barrier coatings, Part II: Active filler loaded SiOC system for superalloys, *Journal of the European Ceramic Society*, 31 (2011) 3011-3020.
- [7] K. Lu, D. Erb, Polymer derived silicon oxycarbide-based coatings, *International Materials Reviews*, 63 (2017) 139-161.

- [8] M. Gunthner, A. Schutz, U. Glatzel, K.S. Wang, R.K. Bordia, O. Greissl, W. Krenkel, G. Motz, High performance environmental barrier coatings, Part I: Passive filler loaded SiCN system for steel, *Journal of the European Ceramic Society*, 31 (2011) 3003-3010.
- [9] M.R. Mucalo, N.B. Milestone, I.C. Vickridge, M.V. Swain, Preparation of Ceramic Coatings from Pre-Ceramic Precursors .1. Sic and Si₃N₄/Si₂N₂O Coatings on Alumina Substrates, *Journal of Materials Science*, 29 (1994) 4487-4499.
- [10] F. Bauer, U. Decker, A. Dierdorf, H. Ernst, R. Heller, H. Liebe, R. Mehnert, Preparation of moisture curable polysilazane coatings Part I. Elucidation of low temperature curing kinetics by FT-IR spectroscopy, *Progress in Organic Coatings*, 53 (2005) 183-190.
- [11] M.R. Mucalo, N.B. Milestone, Preparation of Ceramic Coatings from Pre-Ceramic Precursors .2. Sic on Metal Substrates, *Journal of Materials Science*, 29 (1994) 5934-5946.
- [12] Y.A. M. Gunthner, G. Motz, Polymeric and ceramic like coatings on the basis of SiN(C) precursors for the protection of metals against corrosion and oxidation, *Advanced ceramic coatings and interfaces*, The American Ceramic Society, (2007) 277-284.
- [13] A. Klausmann, K. Morita, K.E. Johanns, C. Fasel, K. Durst, G. Mera, R. Riedel, E. Ionescu, Synthesis and high-temperature evolution of polysilylcarbodiimide-derived SiCN ceramic coatings, *Journal of the European Ceramic Society*, 35 (2015) 3771-3780.
- [14] K.G. Nickel, Corrosion: No Problem for Precursor-Derived Covalent Ceramics?, *Precursor-Derived Ceramics*, (1999).
- [15] N.S. Jacobson, E.J. Opila, K.N. Leeb, Oxidation and corrosion of ceramics and ceramic matrix composites, *Current Opinion in Solid State and Materials Science*, 5 (2001) 301-309.
- [16] G. Chollon, Oxidation behaviour of ceramic fibres from the Si±C±N±O system and related sub-systems, *Journal of European Ceramic Society*, 20 (2000) 1959-1974.

- [17] R. Raj, L. An, S. Shah, Oxidation Kinetics of an Amorphous Silicon Carbonitride Ceramic, *Journal of American Ceramic Society*, 84 (2001) 1803–1810.
- [18] K. Wang, J. Unger, J.D. Torrey, B.D. Flinn, R.K. Bordia, Corrosion resistant polymer derived ceramic composite environmental barrier coatings *Journal of European Ceramic Society*, 34 (2014) 3597-3606.
- [19] M. Bik, M. Stygar, P. Jeleń, J. Dąbrowa, M. Leśniak, T. Brylewski, M. Sitarz, Protective-conducting coatings based on black glasses (SiOC) for application in Solid Oxide Fuel Cells, *International Journal of Hydrogen Energy*, 42 (2017) 27298-27307.
- [20] V.M. Aroutiounian, K. Martirosyan, P. Soukiassian, Almost zero reflectance of a silicon oxynitride/porous silicon double layer antireflection coating for silicon photovoltaic cells, *Journal of Physics D: Applied Physics*, 39 (2006) 1623-1625.
- [21] S. Iwamori, Y. Gotoh, K. Moorthi, Characterization of silicon oxynitride gas barrier films, *Vacuum*, 68 (2003) 113-117.
- [22] N. Takahashi, I. Murakoshi, S. Sasada, The development of the Ceramics Nano-Film Coating having both high corrosion resistance and excellent heat resistance, Yamaha Motor Company, (2010).
- [23] M. Günthner, T. Kraus, W. Krenkel, G. Motz, A. Dierdorf, D. Decker, Particle-Filled PHPS Silazane-Based Coatings on Steel, *International Journal of Applied Ceramic Technology*, 6 (2009) 373-380.
- [24] K.S. Wang, M. Gunthner, G. Motz, B.D. Flinn, R.K. Bordia, Control of Surface Energy of Silicon Oxynitride Films, *Langmuir*, 29 (2013) 2889-2896.

- [25] M. Günthner, K. Wang, R.K. Bordia, G. Motz, Conversion behaviour and resulting mechanical properties of polysilazane-based coatings, *Journal of the European Ceramic Society*, 32 (2012) 1883-1892.
- [26] K.S. Wang, X.H. Zheng, F.S. Ohuchi, R.K. Bordia, The Conversion of Perhydropolysilazane into SiON Films Characterized by X-Ray Photoelectron Spectroscopy, *J Am Ceram Soc*, 95 (2012) 3722-3725.
- [27] L. An, Y. Wang, L. Bharadwaj, L. Zhang, Y. Fan, D. Jiang, Y. Sohn, V.H. Desai, J. Kapat, L.C. Chow, Silicoaluminum Carbonitride with Anomalously High Resistance to Oxidation and Hot Corrosion, *Advanced Engineering Materials*, 6 (2004) 337-340.
- [28] D.J. Young, Chapter 1 - The Nature of High Temperature Oxidation, in: D.J. Young (Ed.) *High Temperature Oxidation and Corrosion of Metals (Second Edition)*, Elsevier, 2016, pp. 1-30.
- [29] N. Birks, G.H. Meier, F.S. Pettit, *Introduction to the High Temperature Oxidation of Metals*, 2 ed., Cambridge University Press, Cambridge, 2006.
- [30] P. Promdirek, G. Lothongkum, S. Chandra-Ambhorn, Y. Wouters, A. Galerie, Oxidation Kinetics of AISI 441 Ferritic Stainless Steel at High Temperatures in CO₂ Atmosphere, *Oxidation of Metals*, 81 (2013) 315-329.
- [31] E.J. Opila, Oxidation and Volatilization of Silica Formers in Water Vapor, *Journal of American Ceramic Society*, 86 (2003) 1238-1248.
- [32] E.J. Opila, N.S. Jacobson, D.L. Myers, E.H. Copland, Predicting Oxide Stability in High-Temperature Water Vapor, *JOM*, (2006) 23-28.

- [33] E.J. Opila, Volatility of Common Protective Oxides in High-Temperature Water Vapor: Current Understanding and Unanswered Questions, *Materials Science Forum*, 461-464 (2004) 765-774.
- [34] J.G. Grolig, J. Froitzheim, J.E. Svensson, Coated stainless steel 441 as interconnect material for solid oxide fuel cells: Oxidation performance and chromium evaporation, *Journal of Power Sources*, 248 (2014) 1007-1013.
- [35] A. Srisrual, S. Coindeau, A. Galerie, J.P. Petit, Y. Wouters, Identification by photoelectrochemistry of oxide phases grown during the initial stages of thermal oxidation of AISI 441 ferritic stainless steel in air or in water vapour, *Corros Sci*, 51 (2009) 562-568.
- [36] D. Bahloul, M. Pereira, P. Goursat, N.S. Choong, K. Yive, R.J.P. Corriu, Preparation of Silicon Carbonitrides from an Organosilicon Polymer .1. Thermal-Decomposition of the Cross-Linked Polysilazane, *J Am Ceram Soc*, 76 (1993) 1156-1162.